

CHARACTERIZATION AND GLOBAL DISTRIBUTION OF A NEW, SPECTRALLY DISTINCT SURFACE FEATURE IN MARS ODYSSEY THEMIS DATA. M. M. Osterloo¹, F. S. Anderson¹, V. E. Hamilton¹, T. D. Glotch², ¹Hawaii Institute of Geophysics & Planetology, University of Hawaii, osterloo@higp.hawaii.edu, ²Jet Propulsion Laboratory, Caltech.

Introduction: We have investigated a series of recently identified, spectrally distinct surfaces exposed predominantly throughout the southern highlands of Mars [1, 2]. The materials of interest are characterized by a distinctive color combination in THEMIS decorrelation stretched images. The material displays a higher band 5 emissivity (1075 cm^{-1}) than the surrounding surfaces in THEMIS IR data and is characterized in TES data by having a distinct slope towards lower wavenumbers (longer wavelengths). Many exposures are spatially small and typically cover less area than a TES pixel ($\sim 3 \text{ km} \times 3 \text{ km}$).

We present here our initial results on the global distribution of these distinct materials as well as a more detailed study of a relatively large occurrence located in the Terra Sirenum region.

Methods: To investigate these interesting materials, we have examined multiple datasets, described below.

THEMIS image processing. We identified these spectrally unique materials using Mars Odyssey Thermal Emission Imaging System (THEMIS) infrared radiance images [3]. The THEMIS IR subsystem images Martian radiance at nine wavelengths ($\sim 1 \mu\text{m}$ wide) from ~ 6 to $14.5 \mu\text{m}$. THEMIS data that are above 220K are processed and displayed as ‘four panel plots’, which are available at the THEMIS data public website (<http://themis-data.mars.asu.edu>). Four panel plots consist of three decorrelation stretched (DCS) images (with band combinations 8/7/5, 9/6/4, and 6/4/2, where the ordered bands are displayed as red, green, and blue respectively) and a brightness temperature image. DCS images help to distinguish differences in generally highly correlated data [4]. The materials of interest appear blue in the 8/7/5 DCS, green in the 9/6/4 DCS, and yellow or orange in the 6/4/2 DCS. We surveyed the four panel plots through orbit 10,300 and logged the localities of these materials.

Spectral properties. THEMIS calibrated radiance data contain a constant atmospheric emission contribution that results in variable effective spectral emissivity from surfaces of different temperatures. A method for removing this atmospheric emission component is described by [5] and has been employed here. We then convert the image to apparent emissivity by finding the highest brightness temperature between bands 3 and 9 (7.9 to $12.6 \mu\text{m}$), and then dividing by the Planck func-

tion that corresponds to that brightness temperature. The apparent emissivity data has a component from atmospheric absorption and scattering, which we correct for using the surface-atmosphere correction method of [5].

The TES instrument provides hyperspectral data at low spatial resolution ($3 \text{ x } \sim 8 \text{ km}$). For a full description of the TES instrument see [6]. To remove atmospheric contributions we utilize the linear deconvolution method of [7,8]. We examined TES data acquired between OCKs (orbital counter keeper) 1683 and 8000. We limited our data to those with average daytime temperatures above 265 K and with incidence angles less than 10° . We also constrained our data to those that had atmospheric dust opacities below 0.15 and water ice opacities less than 0.04.

The spatial scale of the materials of interest are relatively small (at times only filling the field of view of one TES detector), therefore averaging of detectors within an ICK (incremental counter keeper) to reduce noise is not an option as this would minimize the contribution of the materials' spectral signature. We utilize spectral ratios to help isolate the spectral signatures of these deposits in both TES and THEMIS emissivity data [9]. Spectra that are near each other in elevation and location can be ratioed to cancel atmospheric components [9].

Target transformation and factor analysis can help determine the independently varying components in a set of TES data [7,8]. These varying components are commonly atmospheric dust, water ice, and surface composition. Previous studies used this method to isolate hematite [10]. Factor analysis is used to determine the number of independently varying components present in the data set. Target transformation uses the eigenvectors to reconstruct a trial spectrum by applying a linear least squares fit. If the trial spectrum is fit well by the eigenvectors, then that trial spectrum is a potential end member present in the data. If the trial spectrum is not fit well by the eigenvectors, the best fit is commonly close to the actual end member [8]. This analysis technique is commonly used when spectral fitting with end member libraries through linear deconvolution yields inconclusive results.

To investigate the spectral variability within the regions, we employed a number of processing algorithms developed and by RSI and pre-packaged into ENVI . A

pixel purity index (PPI) was applied to a number of THEMIS atmospherically corrected IR emissivity data to identify the extreme pixels within the scene. The PPI was applied to THEMIS data that was processed through a minimum noise fraction (MNF) transformation.

Thermophysical properties. Thermophysical properties of the surface such as thermal inertia and albedo are an integral element in understanding the geology of a region. Thermal inertia is the key factor that controls the diurnal surface temperature variations, and is dependent on the physical properties of the top few centimeters of the surface [11, 12]. The Terra Sirenum example presented below utilizes THEMIS-derived thermal inertia based on the method of [13]. THEMIS nighttime-derived thermal inertia values have an overall accuracy of $\sim 20\%$, a precision of 10-15%, and are consistent with both Thermal Emission Spectrometer (TES) orbital data and Miniature Thermal Emission Spectrometer surface thermal inertia values [13].

We examined Lambert albedo values derived from the TES visible/near IR broadband radiometer (0.3 to 2.9 μm) [6] for any correlation with the locations of these materials. Bright surfaces (albedo >0.20) are generally dust-covered, whereas dark regions (<0.20) are generally non-dusty surfaces. Darker regions commonly have coarser particles and display a variety of spectral features.

In addition to Lambert albedo values, we utilize the dust cover index (DCI) developed by [9]. The DCI identifies surfaces that range from dust covered (DCI <0.940) to dust free (DCI >0.962).

Other datasets. To further aid our understanding of the geologic context of these deposits we also utilized Mars Orbital Camera (MOC) images [14] and Mars Orbital Laser Altimeter (MOLA) data gridded at 128 pixels per degree [15].

Results: Below we discuss the global distribution of the unusual materials, and present a more detailed description of a specific occurrence in Terra Sirenum.

Global distribution. The locations where the materials of interest occur are shown in Figure 1, overlaid on a TES global albedo map. Due to temperature constraints described above, the polar latitudes are under-represented in the THEMIS four-panel plot dataset. This prevents us from investigating high latitudes using this dataset. However, it is evident that the materials of interest are primarily located in the lower albedo southern highland intercrater plains. The deposits are seen in small craters or following irregular outlines, but typically occurs as small ($\sim 1\text{km}^2$ to $\sim 25\text{km}^2$), spatially isolated deposits. They are found in relative lows in comparison to the surrounding region [1,2].

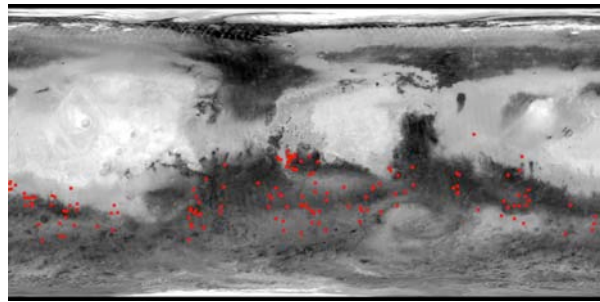


Figure 1. TES global Lambert Albedo map (<http://jmars.asu.edu/data/>) with locations of the materials of interest in red.

Terra Sirenum: A large exposure is located in the Terra Sirenum region of Mars (near $\sim 205^\circ\text{E}$, -33°N) [1]. Figure 2 shows the extent of the deposit in a THEMIS daytime IR DCS mosaic (8/7/5), where the material of interest is shown in the bright blue color. Boxes indicate locations of MOC images (red) and area averaged for spectral analysis (black).

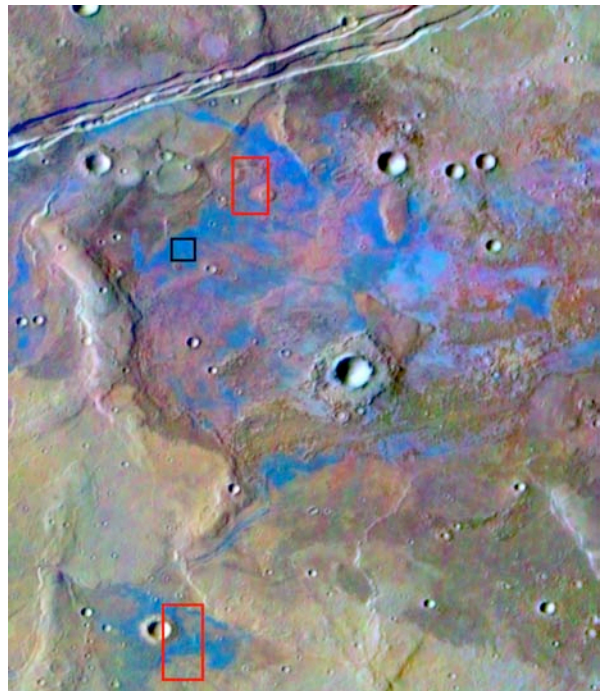


Figure 2. THEMIS IR radiance DCS mosaic of the Terra Sirenum deposit (bounding box ~ 205.20 to 206°E and ~ 32.50 to 31.80°S)

The exposure here is typical of many occurrences; it is located in a relative low (elevations range from ~ 1160 m to 1300 m near the exposures, and outside are ~ 1500 m), abuts craters, and follows irregular paths. Here, the

material also follows Sirenum Fossae but does not cross it. This region in Terra Sirenum appears to have a complex geologic history. MOC images indicate the materials of interest are relatively brighter in tone and have an indurated appearance as shown in Figure 3 (left and right). The circular shapes in the MOC image at left are pedastal craters and the "blue" materials in-fill the low regions near these relative highs. Figure 3 (right) shows another MOC image of the materials underlying the darker toned adjacent materials and following an irregular path to the south.

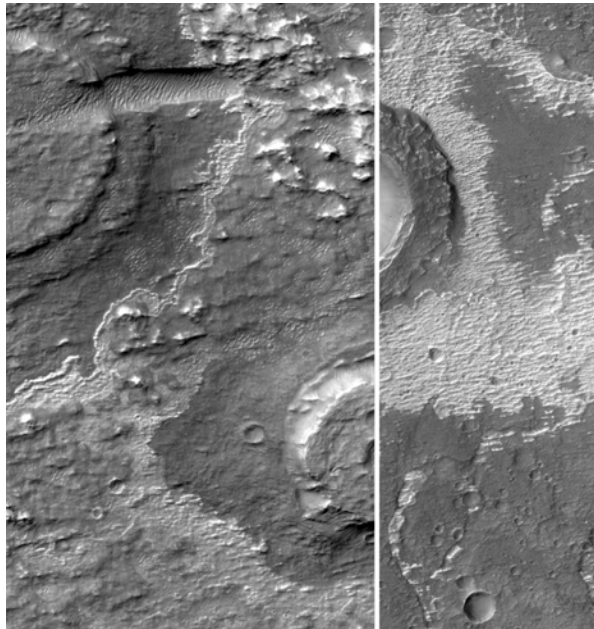


Figure 3. Section of MOC image s1601635 (left) and section of MOC image s1201518 (right) (~3.0 km and ~3.5 km across respectively). Materials of interest are the lighter toned deposits.

TES Lambert albedo values of the unusual materials indicate they are not significantly brighter than the surrounding region (~0.12 to 0.13 in comparison to regional values ranging from ~0.11 to 0.14). THEMIS nighttime thermal inertia values range from ~310 to ~340 $\text{Jm}^{-2}\text{K}^{-1}\text{s}^{-1/2}$ for the materials, although areas that are 'lighter blue' in Figure 2 have lower thermal inertia values (~270 to 290 $\text{Jm}^{-2}\text{K}^{-1}\text{s}^{-1/2}$). In general, the materials have a relatively higher thermal inertia than the surrounding plains with an equivalent particle size of 1-2 mm (coarse sands or indurated material) [16]. DCI values for the area indicate a dust free surface (0.961 to 0.987).

PPI results indicate that the "blue" materials in Figure 2 are among the spectrally pure end members for the scene both in apparent emissivity space as well as

atmospherically corrected emissivity space. Averaged atmospherically corrected THEMIS emissivity spectra from the materials of interest (informally dubbed 'glowing' terrain) have higher emissivities than the surrounding region in bands 4, 5, and 6 (1175, 1075, 984 cm^{-1} respectively). The materials have lower emissivities in bands 8 and 9 (851 and 796 cm^{-1} respectively), although standard deviations typically overlap. The materials are characterized by a higher band 5 (1075 cm^{-1}) emissivity than the surrounding areas and display a distinctly different spectral shape. Figure 4 shows a typical averaged 'glowing' terrain spectrum plotted in blue (outlined in Figure 2 with black box) with the averaged regional spectral shape in grey. Surface types I and II are plotted and offset for reference.

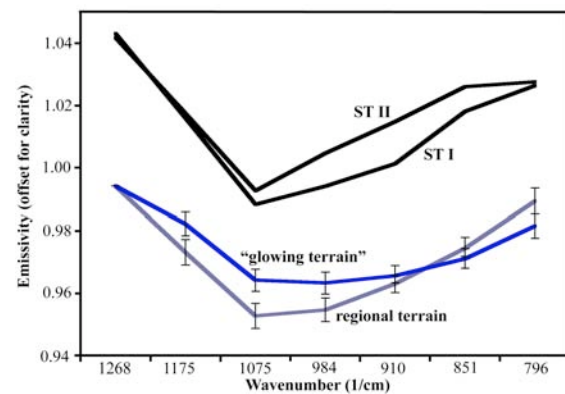


Figure 4. Atmospherically corrected THEMIS emissivity spectra from image I07808003 plotted with surface type I and surface type II.

Initial linear deconvolutions of the TES OCK 4121 over the materials of interest in the Terra Sirenum region yield a surface spectrum that differs from those of the two surface types (ST) originally proposed by [17]. The Terra Sirenum materials appear to have a more subdued spectral characteristic than either ST1 (basaltic) or ST2 (andesitic, weathered basalt [17, 18]) and generally contain a pronounced slope towards longer wavelengths. Linear deconvolutions of single detector spectra of the material of interest, generally model the materials as being composed of pyroxenes (dominantly low Ca pyroxenes), feldspars, and higher abundances of Fe-oxides (primarily as magnetite, with lesser amounts of hematite and goethite), which is consistent with results from [2]. We also retrieved high abundances of halloysite, and smaller abundances of volcanic glasses, smectite clays, olivine, and sulfates (gypsum). The root mean square (RMS) errors for our fits range from 0.22 to 0.33%, which are generally acceptable for single detector deconvolutions. We also

tested an end member set that included a halloysite spectrum from [19], which is a pelletized sample and has deeper spectral features, as well as various sulfate spectra from [20]. The results of these deconvolutions yielded greater oxide abundances (primarily magnetite), less halloysite, and variable amounts of clays and sulfates although all were below detection levels of ~10-15% [21]. The RMS errors from these fits are comparable to those using the initial end member set and are considered equally acceptable.

To further investigate these spectra, we utilized factor analysis and target transformation [12]. We used more than 15 ICKs from OCK 4121 to identify the significant components (eigenvectors) within the data. We used these eigenvectors to model a large and diverse set of trial spectra (the target transformation). No trial spectra (mineral spectra) were fit well, but many minerals have broadly similar shapes and give clues to the spectral shape of the Martian materials. The trial spectra that were best reconstructed and not attributable to atmospheric components included oxides, clays, and sulfates having low contrast spectral features and generally sloping towards lower wavenumbers. These results are in agreement with work from [2] for the materials in other localities.

Spectral ratios of unatmospherically corrected TES data indicate that the main difference between the materials of interest and much of the surrounding terrain is a slope towards lower wavenumbers as shown by [1,2].

Discussion: Linear deconvolution results for the “blue” materials are ambiguous, as shown by the fact that we get acceptable fits with different end member libraries. Factor analysis and target transformation results indicate that no library minerals were fit well [2], though suggest a featureless spectrum that slopes towards lower wavenumbers. Spectral ratios between the material of interest and the outside region also indicate the main difference between the two areas is a slope towards lower wavenumbers. Some minerals such as magnetite exhibit spectral slopes, which is likely why they were chosen in the deconvolution. However, we also investigate the possibility that spectra that appear to have a slope towards lower wavenumbers could be the result of errors in the radiance to emissivity conversion. Unit emissivity in the 1350 – 300 cm^{-1} region is assumed in converting TES radiance to emissivity. If emissivity is not (near) unity in that region [22], or the temperatures of the materials in the field of view are wide-ranging [23], an inaccurate brightness temperature will be used, which can introduce a slope in the resulting emissivity spectrum. There has been no evidence to date that surface temperature variations at TES spatial scales are suffi-

ciently large to produce this effect (though it is known to effect Mini-TES data [23]), so we have focused on the hypothesis that the materials of interest exhibit non-unit maximum emissivity. Most silicates have near-unit or unit maximum emissivity [24, 22]. However, other minerals, such as some oxides [25] and some salts (e.g., halite, sylvite [26]) may not exhibit near-unit emissivity in the wavenumber range used for TES emissivity conversion. If such a mineral were present on the Martian surface in significant abundances (unquantified at present), the assumption of unit emissivity could be violated, and the brightness temperature estimate would be incorrect, leading to the observed spectral slope.

Conclusions: We present a work in progress that indicates a possible new and spectrally distinct surface feature. Relatively higher thermal inertias and slightly higher albedos in comparison to the surrounding terrain indicate the material has distinct thermophysical properties. The material occurs in relative geographic depressions and as shown in MOC data, the material has an indurated appearance and seems to be relatively thin in nature. THEMIS and TES spectral data indicate the material has a distinct spectral shape, which is different from the surrounding plains, as well as previously studied surface types.

References: [1] Osterloo, M. M., et al. (2007) *LPSC XXXVIII* #1814. [2] Glotch, T. D. et al. (2007) *LPSC XXXVIII* #1820. [3] Christensen, P.R. et al. (2004) *SSR*, 110, 85-130. [4] Gillespie, A.R. et al. (1986) *Rem. Sense. Env.*, 20, 209-235. [5] Bandfield, J. L. et al. (2004) *JGR*, 109, E10008. [6] Christensen, P.R. et al (2001) *JGR*, 106, 23823-23871. [7] Smith, M. D. et al. (2000) *JGR*, 105 (E4), 9589-9607. [8] Bandfield, J.L. et al. (2000) *JGR*, 105, 9573-9587. [9] Ruff, S.W. and Christensen, P. R. (2002) *JGR*, 107, E12, 5127. [10] Glotch, T. D. et al. (2004) *JGR*, 109, E7. [11] Mellon, M. T. et al. (2000) *Icarus*, 148, 437-455. [12] Kieffer, H. H. et al. (1977) *JGR*, 82, 4249-4291. [13] Fergason, R.L. et al (2006) *JGR*, 111, E12004. [14] Malin, M. C. and Edgett, K. S. (2001) *JGR*, 106 (E10), 23429-23570. [15] Zuber, M. T. et al. (1992) *JGR*, 97, 7781-7798. [16] Presley, M. A. and Christensen, P. R. (1997) *JGR*, 102, 6551-6566. [17] Bandfield, J. L. et al. (2000) *Science*, 287, 5458. [18] Wyatt, M. B. and McSween, H. Y. Jr. (2002) *Nature*, 417, 263-266. [19] Michalski, J. R. et al. (2006) *JGR*, 111, E03004. [20] Lane, M. D. (2007) *American Mineralogist*, 92, 1, 1-18. [21] Christensen, P. R., et al. (2000) *JGR*, 105, E4, 9609-9621. [22] Ruff, S.W. et al. (1997) *JGR*, 102, B7, 14899-14913. [23] Ruff, S. W. et al. (2006) *JGR*, 111, E12S18. [24] Salisbury, J. W. et al. (1991) *Icarus*, 92, 2, 280-297. [25] Salisbury, J. W. and Wald, A. (1992) *Icarus*, 96, 121-128. [26] Lane, M. D. and Christensen, P. R. (1998) *Icarus*, 135, 528-536.